J-INTEGRAL APPLICATIONS TO CHARACTERIZATION AND TAILORING OF CEMENTITIOUS MATERIALS

VICTOR C. LI
Department of Civil and Environmental Engineering,
University of Michigan
Ann Arbor, MI, 48109-2125

1. Introduction

The J-integral introduced by Professor James R. Rice (Rice, 1968) has found extensive applications in a broad variety of engineering materials. In the last decade, fracture characterization of concrete and deliberate tailoring of fiber reinforced cementitious composites have made great strides. The J-integral has played an important role in these advances. This article reviews the contributions of the J-integral in three distinct but related areas: (a) Characterization of the fracture process of cementitious materials, (b) Testing methodology for the tension-softening constitutive relation in cementitious materials, and (c) Design of cementitious composites with ultra high ductility.

Cementitious materials include a broad variety of engineering materials mostly used in civil engineering applications. These include the ubiquitous concrete made of a composition of aggregates with cement as binder. When the stone aggregates are replaced by sand particles, the composite is referred to as a mortar. Fiber reinforced concrete (FRC) is concrete containing a small amount of fiber, typically less than a few percent by volume, and usually in discontinuous form. In recent years, the trend in high performance cementitious composites has been in the use of mortar as the matrix reinforced with an increasingly broad choice of fiber types. In the early days, high performance cementitious composites are synonymous with high fiber content composites. With improved understanding of the micromechanisms responsible for multiple cracking and pseudo strain-hardening, some of these high performance cementitious composites can now be engineered with only two percent or less of fibers, making them viable economically and processing-wise for use in large scale structural applications. In all of these cementitious materials, a common theme is that the aggregates, sand particles or fibers serve as bridging elements when cracks traverse the cement matrix. The fracture process and mode of failure are strongly influenced by the properties of the bridging tractions working against crack opening and extension.

The non-linear fracture process in concrete is widely accepted in the engineering community, and more accurate prediction of fracture load in concrete elements is now possible. There is a gradually expanding, although still somewhat limited, adoption of fracture based safe design of concrete structural elements. The application of high performance fiber reinforced cementitious composites in load carrying structures is emerging. A rapid growth in this area is expected in the next few years, especially in Japan.

T.-J. Chuang and J.W. Rudnicki (eds.),
Multiscale Deformation and Fracture in Materials and Structures, 385–406.

A detailed account of the fracture processes in cementitious materials can be found in Li and Maalej (1996a,b). The early use of the J-integral for toughness characterization of concrete was proposed by Halvorsen (1980) and Mindess et al (1977).

This article is written in honor of Professor James R. Rice, on the occasion of celebrating his 60th birthday.

2. Fracture Models for Concrete and Fiber Reinforced Cementitious Composites

Hillerborg (1976, 1983) was one of the first to recognize the importance of aggregate bridging in concrete and fiber bridging in FRC in the fracture processes of these material. By including the often large scale process zone as an extension of the traction free crack, the word "fictitious crack" was coined. In order to predict or simulate crack propagation in these materials, fracture models are needed.

Whatever the source of crack face traction is, it is convenient to consider the process zone as the near tip crack segment containing a line of "springs" tying the crack faces. While any spring will invariably resist crack opening, the amount of energy absorption and many macroscopic fracture behavior will depend on the detail behavior of these springs. In general, the springs can be linear or non-linear, hardening or softening. In the case of softening, it can be a result of the same physical process leading to crack tip extension and therefore the presence of the process zone implies cancellation of the crack tip singularity. We refer to such process zone as having 'cohesive' behavior. It is also possible to have the springs and crack tip extension as a result of distinctly different physical processes, as in the case of a fiber reinforced cement. In this case, the spring actions are associated with fiber bridging, whereas the crack tip extension is a result of breaking down of the cement material. We refer to such process zone as having 'bridging' behavior. For a bridged crack, the presence of the bridging zone can co-exist with a crack tip singularity. Such distinction between a *cohesive crack* and a *bridged crack* was first recognized by Cox and Marshall (1994).

Cohesive crack models have been considered in a variety of contexts. Barenblatt (1962) assumed the cohesion on the crack faces to be provided by the forces resisting the separation of the layers of atoms in metals. Rice (1980) studied rock break down at ends of earthquake shear faults. Hillerborg (1983) considered aggregate and ligament bridging in cracked concrete producing a tension-softening behavior. The bridged crack model appears most appropriate for fiber reinforced cementitious materials.

Consider a crack with a process zone of arbitrary size (Fig. 1). Traction in the process zone takes a general relationship between crack face traction versus crack opening $\sigma(\delta)$. The spring law can exhibit hardening and softening, with spring force falling to zero at a critical crack opening δ_t^*. A relationship between such a general spring law and the crack driving force J can be derived by adopting the contours shown in Figure 2, and invoking the path independent property of the J-integral.

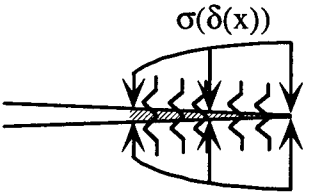

Figure 1. Line-Spring Concept of Process Zone Governing Crack Growth

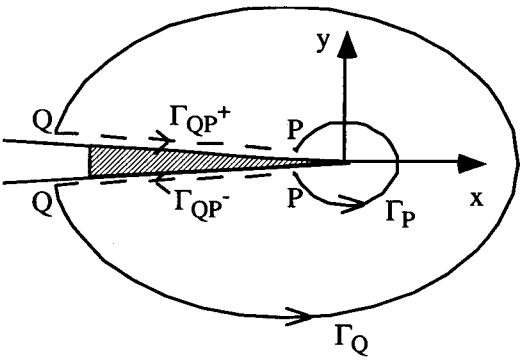

Figure 2. J-integral Contours Chosen for Process Zone Analyses

The result for Mode I is

$$J_{\Gamma_P} = J_{\Gamma_Q} - \int_P^Q \sigma \frac{\partial \delta}{\partial x} dx \tag{1}$$

where δ is the relative crack opening displacement.

We consider three crack models corresponding to different crack tip and spring behavior.

2.1 COHESIVE CRACK MODEL

When the presence of the cohesive zone is a direct result of the crack tip break down process, as is often assumed to be the case in concrete, the crack tip singularity must vanish, i.e.

$$\lim_{\Gamma_P \to tip} J_{\Gamma_P} = 0 \tag{2}$$

Equation (1) then implies

$$J_{\Gamma_Q} = \int_P^Q \sigma \frac{\partial \delta}{\partial x} dx \tag{3}$$

Figure 3 illustrates the tension-softening stress profile σ (x) in the process zone. Note that the stress profile is continuous as it makes the transition from intact material ahead of the fictitious crack tip ($\delta = 0$) to the tension-softening material behind the crack tip.

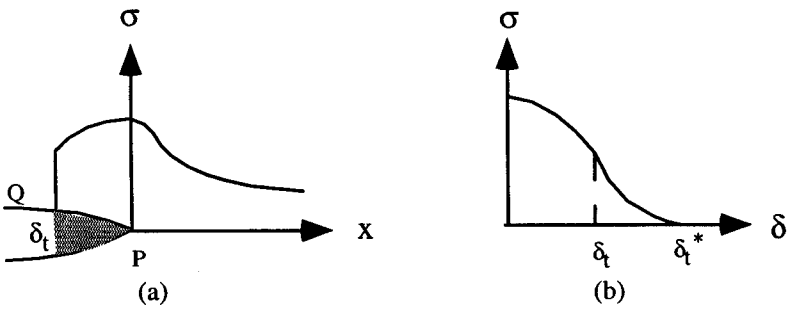

Figure 3. (a) Stress Profile $\sigma(x)$ in Cohesive Crack Model and (b) Corresponding $\sigma(\delta)$ Relationship. Note Crack Opening δ_t at Physical Crack Tip

The integral above can be re-written as

$$J_{\Gamma_Q} = \int_0^{\delta_Q} \sigma d\delta = \int_0^{\delta_t} \sigma d\delta \tag{4}$$

if Q is taken outside the process zone, since for $\delta > \delta_t$, $\sigma = 0$ so that the integration for $\delta > \delta_t$ can be truncated. Because the traction free crack must propagate when the crack mouth opening exceeds δ_t^*, Eqn. (4) affords a definition of the critical J value, or

$$J_c = \int_0^{\delta_t^*} \sigma d\delta \tag{5}$$

Equation (5) denotes an upper limit of J with no restriction on the size of the cohesive zone. It corresponds to the critical value of non-linear fracture parameter J when traction free crack extension initiates. Hence

$$J = J_c \tag{6}$$

with J_c defined in (5) can be considered a crack initiation condition in large scale cohesive zone crack model.

For the special case of small scale 'yielding', i.e. if the process zone is small compared to all other characteristic dimensions in the problem, then J_{Γ_Q} -> G, the standard energy release rate crack driving force parameter. Further, at imminent propagation (δ_t -> δ_t^*), G -> G_C. This affords a physical interpretation of G_C in terms of the inelastic behavior of the process zone material, i.e.,

$$G_c = \int_0^{\delta_t^*} \sigma d\delta \tag{7}$$

or graphically, G_C represents the area under the σ–δ spring law (Fig. 3b).

2.2 BRIDGED CRACK MODEL

For the bridged crack model, the presence of the process zone does not cancel the crack tip singularity. This is the case of fiber reinforced cementitious composites, in which the crack tip singularity can be associated with the fracture toughness of the cement, while fiber bridging provides the spring tractions on the crack wake. Figure 4 illustrates the bridging stress profile $\sigma(x)$ in the process zone. Note that the stress profile is discontinuous as it makes the transition from intact material ahead of the fictitious crack tip to the bridging material behind the crack tip.

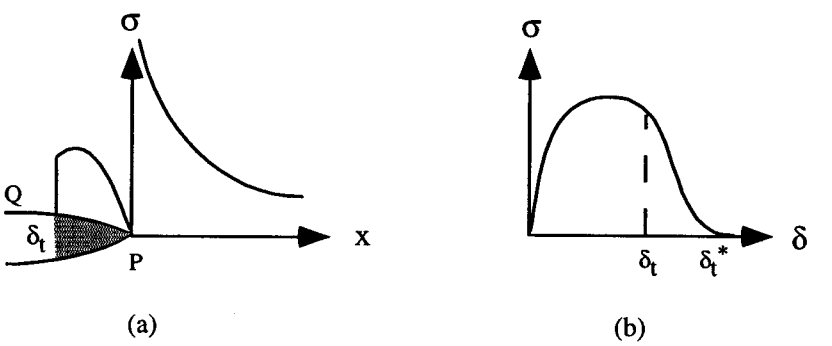

Figure 4. (a) Stress Profile σ (x) in Bridged Crack Model and (b) Corresponding σ (δ) Relationship.

Assuming small scale yielding of the material ahead of the bridging zone, the contour Γ_p can be shrunk onto the crack tip (but remains in the K-dominant zone, assuming that it exists), and we have J_{Γ_P} -> G_c^{tip}, where G_c^{tip} denotes the toughness of the crack tip material independent of the bridging zone processes. Equation (1) then becomes

$$J_{\Gamma_Q} = G_c^{tip} + \int_0^{\delta_t} \sigma d\delta \tag{8}$$

Again, since σ becomes zero when δ_t exceeds δ_t^*, a critical value of J can be defined for extension of the traction free crack:

$$J_c = G_c^{tip} + \int_0^{\delta_t^*} \sigma d\delta \tag{9}$$

For large scale bridging then, crack extension initiates when

$$J = J_c \tag{10}$$

with J_c defined as in (9).

In the case of small bridging length compared to all other length scales in the problem (small scale 'bridging'), J_c and G_c coincides and

$$G_c = G_c^{tip} + \int_0^{\delta_t^*} \sigma d\delta \tag{11}$$

2.3 EMBEDDED PROCESS ZONE MODEL

The Bridged Crack Model discussed above assumes small scale 'yielding' for the crack tip material. However, this does not have to be the case. The recently developed highly ductile Engineered Cementitious Composites (Li and Hashida, 1993) is a good example. In such materials, the fiber bridging zone is embedded inside a volume of material undergoing inelastic deformation (See also Figure 11 in Section 4). This suggests an Embedded Process Zone Model shown schematically in Figure 5 together with a non-linear stress-strain curve depicting the behavior of the inelastic zone (shaded area) embedding the process zone.

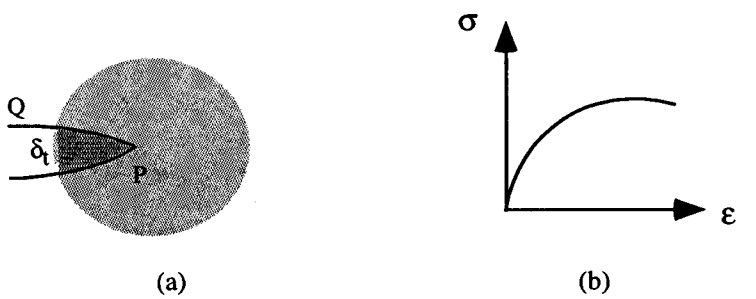

Figure 5. (a) Embedded Process Zone Model, with Inelastic Behavior in Shaded Volume of Material Represented by Non-Linear σ–ε Curve in (b).

Equation (1) then gives

$$J_{\Gamma_Q} = J_m + \int_0^{\delta_t} \sigma d\delta \tag{12}$$

where J_m represents the inelastic energy absorption inside the volumetrically distributed inelastic zone. When both the off-crack-plane inelastic zone and the on-crack-plane (cohesive) process zones are fully developed, the maximum value of J is reached. Thus

$$J_c = J_m + \int_0^{\delta_t^*} \sigma d\delta \tag{13}$$

For most materials best described by the Bridged Crack Model, the crack tip toughness is usually much smaller than the energy consumed in the bridging zone. For materials that can be described by the Embedded Process Zone Model, experimental measurements have indicated a J_m comparable in magnitude to the energy absorbed in the process zone (second term on the right hand side of (13)) (Maalej et al, 1995a).

Again, for large scale process zone embedded inside an inelastic zone, the fracture criterion in terms of J will be

$$J = J_c \tag{14}$$

with J_c defined as in (13).

In the case of small process zone length and small inelastic off-crack-plane zone compared to all other length scales in the problem, J_c and G_c coincides and

$$G_c = G_c^{tip} + \int_0^{\delta_t^*} \sigma d\delta \tag{15}$$

identical to the energy release rate of (11). In this limit, $J_m = G_c^{tip}$.

3. J-Based Fracture Testing in Tension-Softening Material

It can be seen from the above discussion on fracture process characterization that the $\sigma(\delta)$ curve plays an important role as constitutive relation of the line-springs in the fracture process zone. It is therefore important to have experimental methodology or micromechanics based modeling to determine $\sigma(\delta)$. In the following, an experimental technique (Li et al, 1987; Leung and Li, 1989; Hashida et al, 1993; Li et al, 1994) for the determination of $\sigma(\delta)$ taking advantage of the J-integral is briefly reviewed. Micromechanics based modeling of $\sigma(\delta)$ for various fiber reinforced cementitious materials can be found in Li and co-workers (1992, 1995, 1996, 1997).

The experimental technique to be discussed is based on the Compliance Test, first used by Landes and Begley (1972) for elastic-plastic metallic materials, and utilizes the interpretation of J as the difference in potential energy for a differential change in crack length:

$$J = -\frac{1}{B}\frac{\partial(PE)}{\partial a} \tag{16}$$

where B is the specimen thickness. Because crack length change is often difficult to measure, we use a pair of specimens identical in every respect except for a small difference in crack length. The test can be carried out with any specimen geometry, and the resulting value of J_c should in principle be the same. The compact tension specimen can be a convenient choice.

Suppose the two specimens have initial crack lengths of a_1 and a_2, where a_2 is slightly larger than a_1. For a valid test, a_2-a_1 should be smaller than all other dimensions in the specimen, including the thickness B.

The load P and load point displacement Δ are measured for each specimen (Fig. 6a). Due to process zone growth, the P – Δ curve can be nonlinear. Obviously the specimen with longer crack will have larger displacement value for a given load level (more compliant). For any fixed Δ, the area between these two curves may be interpreted as

$$Area(\Delta) = J(a_2 - a_1)B \tag{17a}$$

so that

$$J = \frac{Area(\Delta)}{(a_2 - a_1)B} \tag{17b}$$

Since a_1, a_2 and B are known *a priori* , J can be calculated for each value of Δ. This is shown in Fig. 6b as a J – Δ curve. The plateau value of J is interpreted as the J_C value associated with the full development of the process zone.

During specimen loading, the crack tip opening displacement is also monitored. Thus a triplet of Load P, Load-point displacement Δ, and crack tip displacement δ_t is recorded during the test, and the specimens are loaded to beyond the peak load into the softening regime. Figure 6c shows a Δ versus δ_t correlation curve.

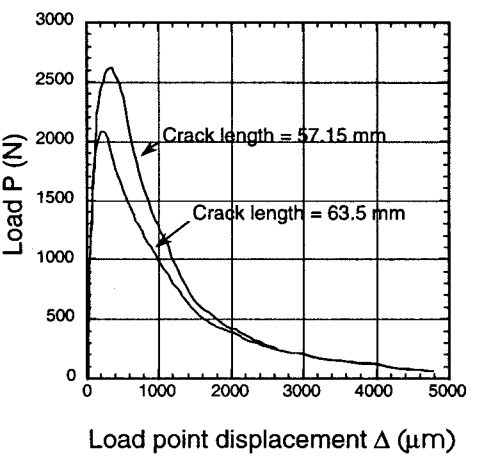

Figure 6a. P – Δ Record for an FRC Specimen (after Li and Ward, 1989)

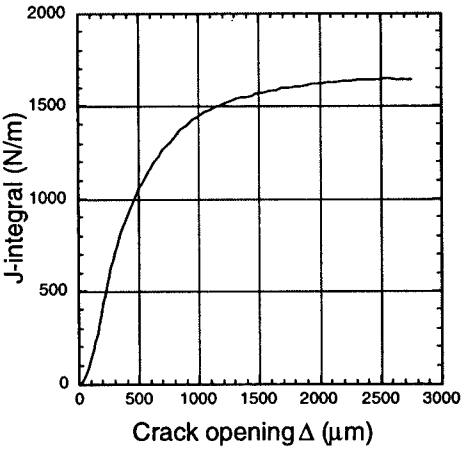

Figure 6b: J – Δ Record

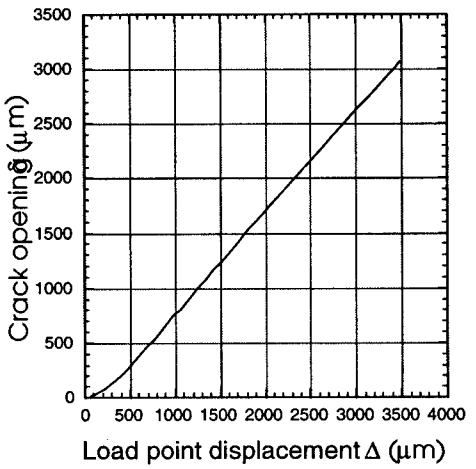

Figure 6c. Δ – δ_t Record

The correlation between Δ and δ_t were used by Li and co-workers to deduce the σ–δ curve. By using the relationship between J and σ(δ) (Equation (4)) for tension-softening materials, the σ–δ curve (Fig. 7) can be obtained by differentiation. That is,

$$\sigma(\delta_t) = \frac{dJ}{d\delta_t} \tag{18}$$

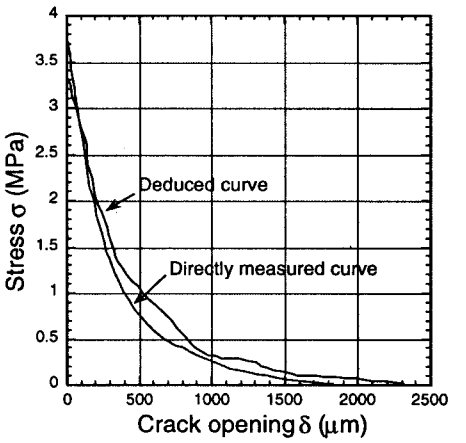

Figure 7. Deduced Tension-Softening Curve

Figure 7 also shows the tension-softening curve of the same FRC material obtained from a uniaxial direct tension test. The good comparison of the two σ–δ curves suggests the accuracy of the J-based testing technique. The J-based method is particularly suitable for brittle materials with sharp dropping σ–δ curves for which the direct tension test may be difficult to carry out due to load instability beyond peak. The J-based testing technique was originally developed for mortar and concrete (Li et al, 1987; Teramura et al, 1990), but has since been applied to fiber reinforced composites (Leung and Li, 1989; Rokugo et al, 1989; Li et al, 1994; Hashida et al, 1994), and rocks (Chong et al, 1989; Hashida, 1990). The J-based technique has been extended to σ–δ relationship determination for materials in which the crack tip singularity is not canceled (Li et al, 1994).

4. Steady State Cracking and Strain-Hardening Design

Although most cementitious materials are considered brittle (e.g. cement), or quasi-brittle (e.g. concrete and FRC), it is possible to design cementitious composites with extremely ductile behavior. One such material, known as Engineered Cementitious Composite (ECC for short), exhibits tensile strain capacity up to 7.5% (Li et al, 1996). The design of such materials is based on the J-integral analyses of steady state cracking and the micromechanics of fiber bridging.

In order to achieve the desirable pseudo-strain hardening behavior, two criteria must be satisfied (Li and Leung, 1992; Li et al, 1996): (i) steady state cracking criterion, and (ii) first crack criterion, which requires the first cracking stress to be lower than the maximum fiber bridging stress. Additional cracks (multiple cracking) can then form on further loading.

The steady state criterion has been studied by a number of researchers, (see, e.g. Marshall and Cox (1988); Li and Wu, (1992); and Li and Leung, (1992)). In fiber composites, the extension of a matrix crack is accompanied by fiber bridging across the

crack flanks. As the matrix crack extends, the bridging zone increases in length. During crack opening, the bridging stress increases as fiber/matrix interfaces debond and the debonded segments of fibers stretch (hardening spring behavior). When the bridging stress increases to the magnitude of the applied load, the crack flanks flatten to maintain the constant applied stress level (Li and Wu, 1992). This load level is termed the steady state cracking stress σ_{SS}.

Based on a J-integral analysis of a steady state crack, Marshall and Cox (1998) showed that

$$J_{tip} = \sigma_{ss}\delta_{ss} - \int_0^{\delta_{ss}} \sigma(\delta)d\delta \tag{19}$$

where J_{tip} refers to the crack tip toughness. In most fiber reinforced cementitious composites with less than 5% fiber volume fraction, J_{tip} can be approximated as the cementitious matrix toughness. The steady state stress σ_{SS} and the flattened crack opening δ_{SS} are related via the bridging law $\sigma(\delta)$. The right hand side of (19) is known as the complementary energy of fiber bridging, and corresponds to the shaded area above the $\sigma(\delta)$ curve in Fig. 8. For steady state cracking to occur at all, the steady state cracking stress must be less than the maximum bridging stress σ_O in the bridging law. That is,

$$\sigma_{ss} \leq \sigma_o \tag{20}$$

Equation (19) and (20) together imply

$$J_{tip} \leq \sigma_o\delta_o - \int_0^{\delta_o} \sigma(\delta)d\delta \tag{21}$$

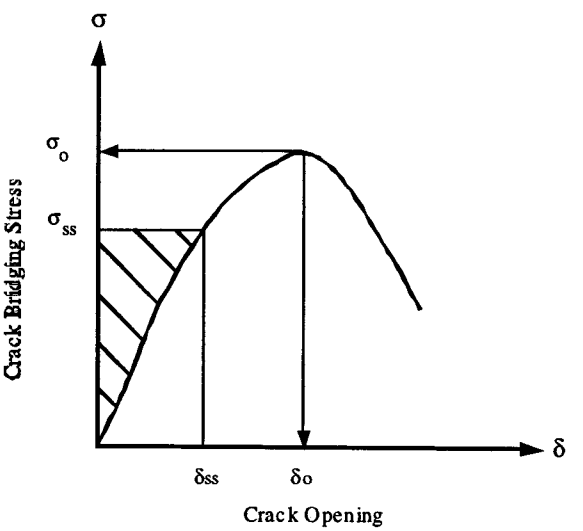

Figure 8. Complementary Energy Concept of Fiber Bridging

Equation (21) provides a general condition for transition from quasi-brittle to strain-hardening failure mode, and highlights the importance of the total complementary energy (right hand side of (21)) in composite design.

For Eqn. (21) to be useful in fiber, matrix and interface tailoring, it will be necessary to determine the bridging law $\sigma(\delta)$ specific for a given composite system. In fiber reinforced cementitious composites in which the fibers are randomly oriented and in which pull-out (rather than fiber rupture) are expected, the bridging laws developed by Li and Leung (1992) can be summarized in the following form:

$$\sigma(\delta)=\begin{cases}\sigma_o\left[2(\delta/\delta_o)^{1/2}-(\delta/\delta_o)\right] & \text{for } \delta\le\delta_o\\ \sigma_o\left(1-2\delta/L_f\right)^2 & \text{for } \delta_o\le\delta\le L_f/2\\ 0 & \text{for } L_f/2\le\delta\end{cases} \tag{22}$$

where $\delta_o = \tau L_f^2/[E_f d_f (1+\eta)]$ is the crack opening corresponding to the maximum bridging stress

$$\sigma_o=\frac{1}{2}g\tau V_f\frac{L_f}{d_f} \tag{23}$$

Corresponding equations for cases where fibers can rupture and for cases where fibers are of variable diameters can be found in Maalej et al (1995b), and Li and Obla (1996). In Eqs. (22) and (23), V_f, L_f, d_f, and E_f are the fiber volume fraction, length, diameter and Young's Modulus, respectively. τ is the fiber/matrix interface friction, and the snubbing factor

$$g=\frac{2}{\left(4+f^2\right)}\left(1+e^{f\pi/2}\right) \tag{24}$$

where f is a snubbing coefficient which must be determined experimentally for a given fiber/matrix system (Li et al, 1990). The snubbing coefficient raises the bridging stress of fibers bridging at an angle inclined to the matrix crack plane, appropriate for flexible fibers exiting the matrix analogous to a rope passing over a friction pulley. Finally, $\eta = (V_f E_f)/(V_m E_m)$, where V_m and E_m are the matrix volume fraction and Young's Modulus, respectively.

The condition for steady state cracking expressed in Eqn. (21) can now be interpreted as a critical fiber volume fraction above which the composite will show pseudo strain-hardening. Using (22) in (21), this critical fiber volume fraction can be defined in terms of the fiber, matrix and interface parameters (Li and Wu, 1992):

$$V_f^{crit} \equiv \frac{12 J_{tip}}{g\tau\left(L_f / d_f\right)\delta_o} \tag{25}$$

Equation (25) is important for composite design. It provides guidelines for tailoring the microparameters such that V_f^{crit} is minimized (Li, 1998). Strain-hardening composites can then be designed with the minimum fiber content.

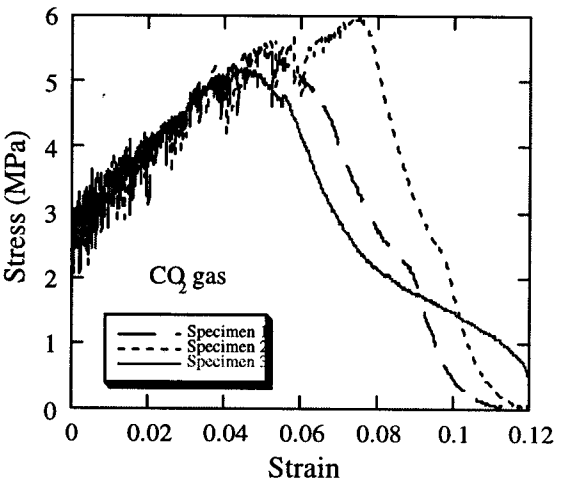

Figure 9. Uniaxial Tensile Stress-Strain Curve of an ECC with CO_2 gas plasma treated PE fibers

In what follows, we describe the mechanical properties for an ECC. Unless otherwise stated, the ECC referred to contains two volume percent of polyethylene fibers. Using Eq. (25) and appropriate parametric values (see Li, 1998), the critical fiber volume fraction is estimated to range between 0.5% and 1%. Hence a composite with 2% fiber should satisfy the condition of pseudo strain-hardening, and exhibit high strain capacity after first cracking.

Figure 9 shows the stress-strain curves from uniaxial tension tests. The ECC strain hardens to an average strain at peak stress ε_{cu} approximately equal to 5.6 % (about 560 times the strain capacity of the unreinforced matrix). For this composite, real-time observation showed that multiple cracking occurred with many sub-parallel cracks across the specimen during strain-hardening. Beyond peak stress, localized crack extension occurred accompanied by fiber bridging. The multiple cracking pattern of a specimen is shown in Figure 10.

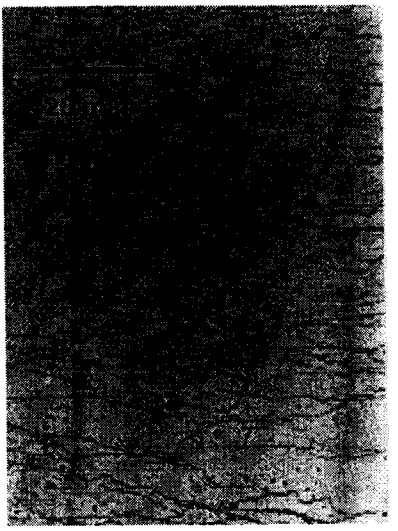

Figure 10. Multiple Crack Pattern of an ECC at About 4.2% Tensile Strain

The total fracture energy of ECC was determined (Li and Hashida, 1993; Maalej et al, 1995) by means of the J-based technique (Eqn. 17b) and using a set of DCB specimens with different notch lengths. Concurrently with the tests, damage evolution on the specimen surface was recorded using a camera.

Figure 11 presents the damage evolution recorded at various loading stages. It is particularly noted that an extensive microcrack damage zone spreads around the notch tip before the localized crack starts to grow. Significant energy absorption is therefore expected from the off-crack-plane volumetric inelastic deformation process. The total fracture energy measured for this ECC was 27 kJ/m^2, with approximately over half of this energy consumed in the inelastic damage process occupying an area of 1150 cm^2 around the crack tip, and the rest coming from the pull-out of fibers on the crack wake. For the ECC, the Embedded Process Zone Model discussed in Section 2.3 is most appropriate in describing its fracture process.

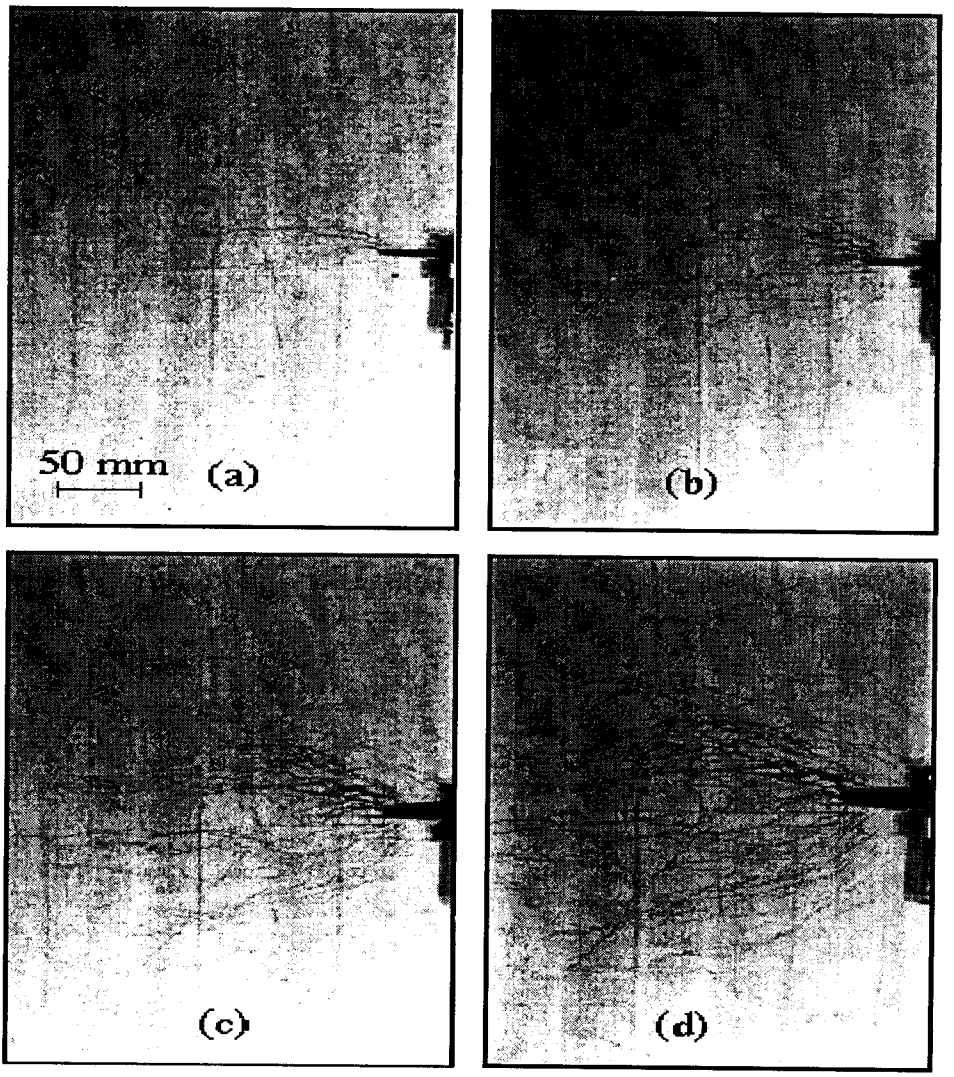

Figure 11. DCB Specimen Showing Evolution of Notch Tip Inelastic Zone at Four Loading Stages.

The notch-sensitivity of ECC has been examined with double edge notched specimens. Test results are shown in Figure 12, which plots the peak load as a function of the reduced section of the notched specimens. The data of the notched specimen lying near (and actually slightly above) the linear line suggests that these composites are notch-insensitive. The surface of the notched specimen (Fig. 13) shows multiple cracks typical of strain hardening fiber reinforced composites. Although the ultimate localized fracture is in the reduced section, multiple cracking spreads along the full length of the specimens prior to final failure. These results suggest that highly damage tolerant structural behavior can be achieved.

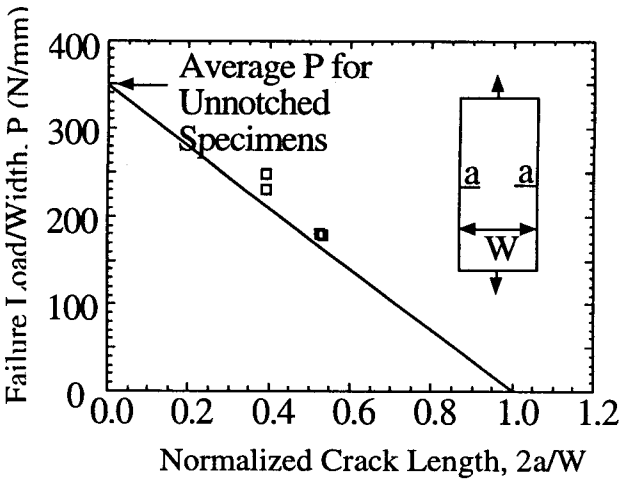

Figure 12. Nominal Failure Load of Double Edged Notch Specimen

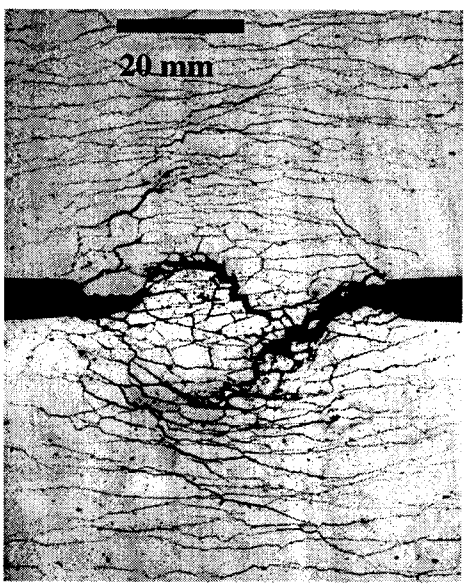

Figure 13. Damage Pattern of DEN Specimen

The ability of ECC to deform non-linearly with strain-hardening in tension combined with high damage tolerance suggests its use in concrete elements which require bolt jointing. An experimental study (Li and Kanda, 1998) was carried out to determine the

response of an ECC slab under circular indentor load (Fig. 14). For this ECC material, 1.25% of PVA fiber was employed. In uniaxial tension the strain capacity was 5%. As control, a similar slab with plain mortar was tested under the same load configuration. Three different size indentors were used. Figure 15 shows the load-deformation (indentor deflection) curves for the ECC and the mortar specimens (used as control). Each specimen type was loaded with three bearing sizes expressed as a percentage of slab surface area. While the load capacity in each case is comparable, it is clear that the deformation capacity of the ECC slab is about one order of magnitude higher than that of the mortar slab at failure.

Figure 16 shows the failure pattern of a mortar specimen, which fractures brittlely into several pieces as expected. The corresponding failure of the ECC specimen is much more ductile. Even as the indentor penetrates the surface of the slab, the surrounding material undergoes inelastic damage with no fractures (Figure 17a). Figure 17b gives an enlarged view of the indentor punch.

The results of this test confirms the notion that the strain-hardening and damage tolerance of ECC can be very effective in alleviating the high stress concentrations experienced by structural elements whenever steel and concrete materials come into contact with each other. Such elements may include concrete embedded steel anchors, and connections in hybrid concrete/steel structural members.

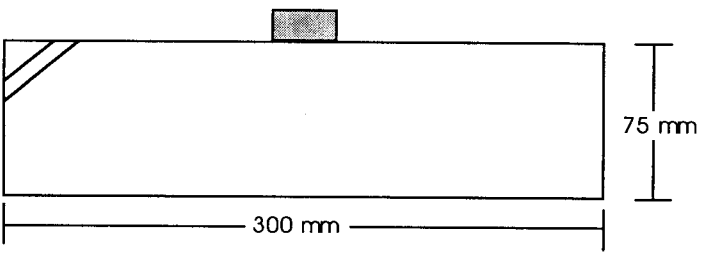

Figure 14. Geometry of indentor and ECC/Mortar Slab

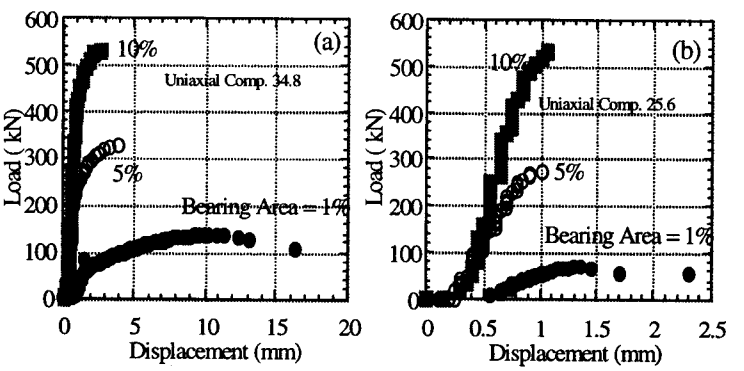

Figure 15. Load -Deformation Curves for (a) Mortar, and (b) ECC Slab

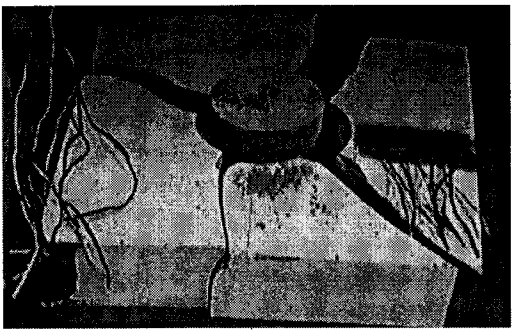

Figure 16. Fracture Failure Pattern of A Mortar Specimen

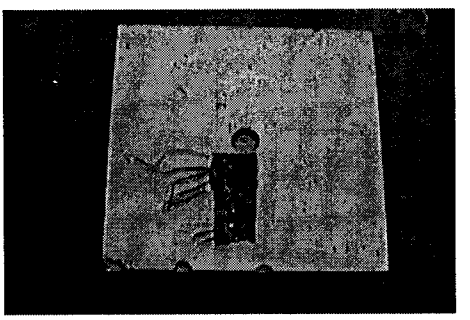

(a)

(b)

Figure 17. (a) Ductile Indented Pattern of A ECC Specimen, and (b) Enlarged View

ECC is now being investigated for structural applications (Li and Kanda, 1998; Fukuyama et al, 1999; Parra-Montesinos and Wight, 2000). A recent study (Fischer and Li, 2000) on exploiting the strain-hardening and multiple cracking behavior of ECC in highly earthquake resistant building systems involves fully reversed cyclically loaded flexural members. These flexural members are made of ECC reinforced with longitudinal steel or FRP rods. Figure 18 shows the deformed shape of an ECC/aramid-FRP element at 10% interstory drift. Microcracks less than 200μm are formed along the full length of the element. The corresponding hysteretic loops indicating large deformation capacity but with low residual deformation (especially for drift less than 5%) are also shown. In contrast to typical concrete/steel element behavior, no spalling of the ECC matrix or buckling of the axial reinforcements are observed. Corresponding tests with ECC/steel elements show extremely high energy absorption behavior (Fischer and Li, 2000). These characteristics can be used to design building systems with high safety as well as minimal post-earthquake repair needs.

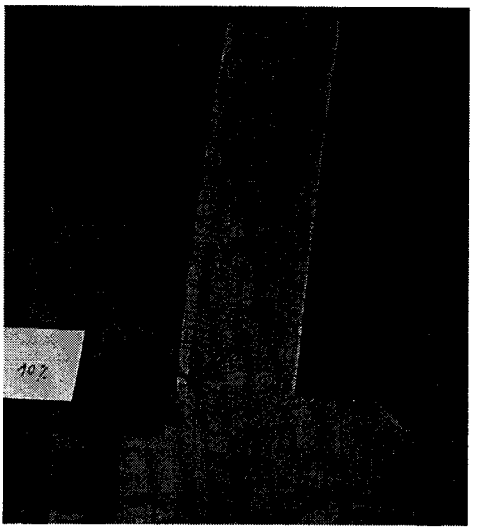

(a)

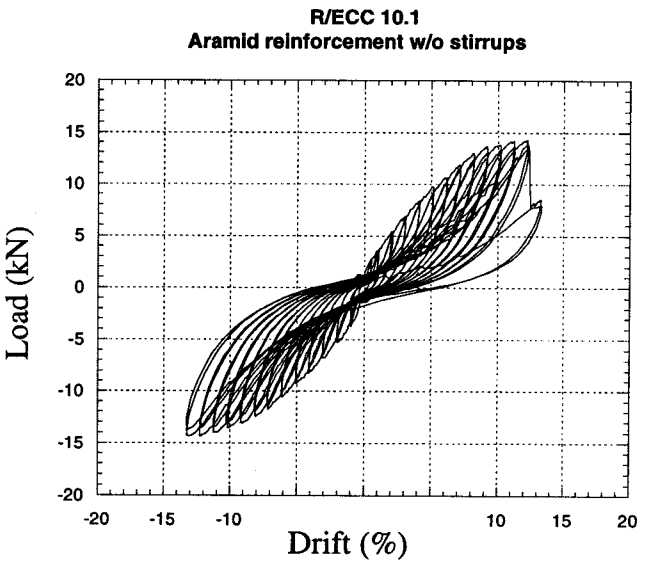

(b)

Figure 18. (a) FRP Reinforced ECC Flexural Element at 10% drift and (b) load deformation behavior

5. Conclusions and Further Discussions

The J-integral has played an important role in the understanding of the mechanics and the engineering of the composites of cementitious materials. This article reviews the use of the J-integral in fracture process characterization, tension-softening curve determination, and microstructural tailoring of cementitious materials. Advancements in these areas provide important tools for failure analyses of structures of cementitious materials, as well as tools for cementitious composite design for safe structures.

Before closing, we note an often misdirected criticism of the application of the J-integral to tension-softening materials. The criticism is directed at the fact that since the J-integral rests on the assumption of non-linear elasticity, and since the process zone material softens inelastically, the application of the J-integral to tension-softening materials cannot be valid. The apparent paradox is resolved if it is understood that the J-integral contour (see, e.g. the contours Γ_{QP+} and Γ_{QP-} in Fig. 2) is placed in the elastic material adjacent to a line of springs (representing the softening material) which can unload. Then the unloading of the springs (softening branch of the σ–δ curve) during crack opening causes a corresponding *elastic* unloading of the material in which the contour is placed. This can be better envisioned with a tensile specimen of a quasi-brittle material. Once a localized fracture zone is formed, the material in the fracture zone unloads (inelastically), while to maintain equilibrium, the material outside the fracture zone, which remains elastic also unloads, but unloads elastically. This phenomenon was nicely illustrated with concrete specimens in uniaxial tensile experiments carried out by Petersson (1981). The strain/displacement gage across the fracture zone shows inelastic unloading (stress drop with increase in crack opening), but the gages outside the fracture zone unloads elastically (decreasing stress with decreasing strain deformation retracing the elastic loading). Hence for the application of the J-integral to tension-softening materials, there is no violation of the requirement of the J-integral as long as the unloading of the material outside the line-spring is elastic.

References

Barenblatt, G. I. (1962) The mathematical theory of equilibrium cracks in brittle fracture, *Advanced Applied Mechanics* **7**, 55-125.

Chong, K.P., Li, V.C., and Einstein, H.H. (1989) Size effects, process zone, and tension softening behavior in fracture of geomaterials, *International J. of Engineering Fracture Mechanics* **34(3)**, 669-678.

Cox, B. and Marshall, D. (1994) Concepts in the fracture and fatigue of bridged cracks, Overview No 111. *Acta Meta. Mate.* **42**, 341-363.

Fischer, G. and Li, V.C. (2000) Structural composites with ECC, to appear in the Proceedings of the ASCCS-2000.

Fukuyama, H., Y. Matsuzaki, K. Nakano, and Y. Sato (1999) Structural Performance of Beam Elements with PVA-ECC, in H. Reinhardt and A. Naaman (eds.), *Proc. of High Performance Fiber Reinforced Cement Composites* 3 (HPFRCC 3), Chapman & Hall, pp. 531-542.

Halvorsen, G.T. (1980) J-integral study of steel fiber reinforced concrete, *International J. Cement Composites*, **2(1)** 13-22.

Hashida, T. (1990) Evaluation of fracture processes in granite based on the tension-softening model, In S.P. Shah, S.E. Swartz & M.L. Wang (eds), Micromechanics of Failure of Quasi-Brittle Materials, *Elsevier Applied Science, London,* 233-243.

Hashida, T., Li, V.C., and Takahashi, H. (1994) New development of the J-based fracture testing technique for ceramic matrix composites, *J. American Ceramic Society* **77(6)**, 1553-1561.

Hillerborg, A. (1983) Analysis of One Single Crack, in F.H. Wittmann (ed.) *Fracture Mechanics of Concrete*, Elsevier Science Publisher, B.V., Amsterdam, pp. 223-250.

Hillerborg, A., Modeer, M., and Petersson, P. E. (1976) Analysis of crack formation and crack growth in concrete by means of fracture mechanics and finite elements. *Cement and Concrete Research* **6**, 773-782.

Landes, J.D. and Begley, J.A. (1972) The Effect of Specimen Geometry on J_{IC}, in *Stress Analysis and Growth of Cracks*, ASTM STP 514, ASTM, Philadelphia

Leung, C.K.Y., and Li, V.C. (1989) Determination of fracture toughness parameter of quasi-brittle materials with laboratory-size specimens, *J. Materials Science* **24**, 854-862.

Li, V.C. (1992) Post-crack scaling relations for fiber reinforced cementitious composites", ASCE *J. of Materials in Civil Engineering*, **4(1)**, 41-57.

Li, V.C. (1998) Engineered Cementitious Composites – Tailored Composites Through Micromechanical Modeling, in N. Banthia, A. Bentur, A. and A. Mufti (eds.) *Fiber Reinforced Concrete: Present and the Future*, Canadian Society for Civil Engineering, Montreal, pp. 64-97.

Li, V.C., Chan, C.M., and Leung, C.K.Y. (1987) Experimental determination of the tension-softening curve in cementitious composites, *J. Cement and Concrete Research* 17-3, 441-452.

Li, V.C. and Leung, C.K.Y. (1992) Steady state and multiple cracking of short random fiber composites, ASCE *J. of Engineering Mechanics* **118(11)**, 2246-2264.

Li, V.C. and Hashida, T. (1993) Engineering ductile fracture in brittle matrix composites, *J. of Materials Science Letters* **12**, 898-901.

Li, V.C. and Kanda, T. (1998) Engineered cementitious composites for structural applications, *ASCE J. Materials in Civil Engineering* **10(2)**, 66-69.

Li, V.C. and Maalej, M. (1996a) Toughening in cement based composites, Part I: Cement, mortar and concrete, *J. of Cement and Concrete Composites* **18(4)**, 223-237.

Li, V.C. and Maalej, M. (1996b) Toughening in cement based composites, Part II: Fiber reinforced cementitious composites, *J. of Cement and Concrete Composites* **18(4)**, 239-249.

Li, V.C., Maalej, M., and Hashida, T. (1994) Experimental determination of stress-crack opening relation in fiber cementitious composites with crack tip singularity, *J. Materials Science* **29**, 2719 - 2724.

Li, V.C., Mihashi, H., Wu, H.C., Alwan, J., Brincker, R., Horii, H., Leung, C., Maalej, M., and Stang, H. (1996) Micromechanical models of mechanical response of HPFRCC, in A.E. Naaman and H.W. Reinhardt (Eds.) *High Performance Fiber Reinforced Cementitious Composites*, RILEM Proceedings 31, pp. 43-100.

Li, V.C. and Obla, K. (1996) Effect of fiber diameter variation on properties of cement based matrix fiber reinforced composites, *Composites Engineering International Journal* **Part B 27B**, 275-284.

Li, V.C. and Ward, R. (1989) A novel testing technique for post-peak tensile behavior of cementitious materials, in H. Mihashi, H. Takahashi, and F.H. Wittmann (eds.) *Fracture Toughness and Fracture Energy – Test Methods for Concrete and Rock*, Balkema, Rotterdam, pp. 183 – 195.

Li, V.C., Wang, Y., and Backer, S. (1990) Effect of inclining angle, bundling, and surface treatment on synthetic fiber pull-out from a cement matrix, *J. Composites* **21(2)**, 132-140.

Li, V.C. and Wu, H.C. (1992) Conditions for Pseudo strain-hardening in fiber reinforced brittle matrix composites, *J. Applied Mechanics Review* **45(8)**, 390-398.

Li, V.C., Wu, H.C., and Chan, Y.W. (1996) Effect of plasma treatment of polyethylene fibers on interface and cementitious composite properties, *J. of American Ceramics Society* **79(3)**, 700-704.

Lin, Z. and Li, V.C. (1997) Crack bridging in fiber reinforced cementitious composites with slip-hardening interfaces, *J. Mechanics and Physics of Solids* **45(5)**, 763-787.

Maalej, M., Hashida, T., and Li, V.C. (1995a) Effect of fiber volume fraction on the off-crack-plane fracture energy in strain-hardening engineered cementitious composites, *J. Amer. Ceramics Soc.* **78(12)**, 3369-3375.

Maalej, M., Li, V.C., and Hashida, T. (1995b) Effect of fiber rupture on tensile properties of short fiber composites, *ASCE J. Engineering Mechanics* **121(8)**, 903-913.

Marshall, D.B. and Cox, B.N. (1988) A J-integral method for calculating steady-state Matrix Cracking Stresses in Composites, *Mechanics of Materials* **7**, 127-133.

Mindess, S., Lawrence, Jr., F.V. and Kesler, C.E. (1977) The J-integral as a fracture criterion for fiber reinforced concrete, *Cement and Concrete Research*, **7**, 731-742.

Parra-Montesinos, G.J., and J.K. Wight (2000) Behavior and Strength of RC Column-to-Steel Beam Connections Subjected to Seismic Loading, to appear in the Proceedings of the 12th WCEE.

Petersson, P-E, (1981) *Crack Growth and Development of Fracture Zones in Plain Concrete and Similar Materials*, Report TVBM-1006, Lund, Sweden, 174pp.

Rice, J. R. (1968) A path-independent integral and the approximate analysis of strain concentration by notches and cracks. *J. Applied Mechanics* **35**, 379.

Rice, J.R. (1980) The mechanics of earthquake rupture, in A.M. Dziewonski and E. Boschi (eds.) *Physics of the Earth's Interior*, Italian Physical Society/North Holland, Amsterdam.

Rokugo, K., Iwasa, M., Seko, S., and Koyanagi, W. (1989) Tension-softening diagams of steel fiher reinforced concrete. In S.P. Shah, S.E. Swartz & B. Barr (eds.), *Fracture of Concrete and Rock, Recent Developments*, pp. 513-522.

Teramura, S., Normura, N., Hashida, T., and Mihashi, H. (1990) Development of a core-based testing method for determining fracture energy and tension-softening relation of concrete, in S.P. Shah, S.E. Swartz and M. L. Wang (eds.), *Micromechanics of Failure of Quasi-Brittle Materials*, Elsevier Applied Science, London, pp. 463-473.